

A Theoretical Prediction on the Intrinsic Half-Metallicity in the Surface-Oxygen-Passivated Cr₂N MXene

Guo Wang

Department of Chemistry, Capital Normal University, Beijing 100048, China

Email: wangguo@mail.cnu.edu.cn

ABSTRACT: Two-dimensional Cr₂N MXene as well as the surface-passivated Cr₂NF₂, Cr₂N(OH)₂ and Cr₂NO₂ are investigated by using density functional theory. The Cr₂N is an anti-ferromagnetic metal. The F atom or OH group-passivation does not change the anti-ferromagnetic characteristics. However, Cr₂NO₂ has a ferromagnetic ground state, which is a half-metal. The half-metallicity of Cr₂NO₂ is still robust when bias is applied to the nanometer sized device. The half-metallicity is intrinsic and does not require atomically clean surfaces. Therefore the stable surface-oxygen-passivated MXene is a good candidate for spintronics.

Keywords: Cr₂N; MXene; half-metallicity; surface-passivation; density functional theory.

INTRODUCTION

The MAX phases are ternary carbides and nitrides with the formula $M_{n+1}AX_n$ ($n=1-3$), in which A is an A-group element and M is a transition metal element. They combine several outstanding properties of metals and ceramics, such as readily machinable (with hack-saw), high damage tolerance, high electrical conductivity, as well as high-temperature oxidation resistance, making them potential candidates for many applications.¹ The MAX phases are hexagonal layered materials, which have two-dimensional characteristics. Usually, the properties of two-dimensional monolayer, such as graphene, are drastically different from those of bulk materials.² In the MAX phases, the A-group elements are weakly bonded and reactive. The A-group can be selectively etched and then graphene-like MXenes can be exfoliated.³ Because of the unique structures, MXenes have potential applications in sensors, catalysts and electrochemical energy storage.⁴

Recent theoretical investigations indicate that several MXenes,⁴ such as Ti_3C_2 ,⁵⁻⁷ Ti_3N_2 ,⁵ Ti_3CN ,⁷ Ti_2C , Ti_2N ,^{8,9} Ta_3C_2 ,¹⁰ Cr_2C and Cr_2N ,¹¹ as well as MXene nanoribbons¹² have magnetic ground states. They have interesting magnetism-related properties, such as half-metallicity of Cr_2C ¹³ and near half-metallicity of Ti_2C and Ti_2N .⁹ For Ti_2C , the structure becomes a true half-metal with a minority-spin gap of 0.04 eV under a biaxial strain.⁹ Moreover, Cr_2C has intrinsic half-metallicity with a large minority-spin gap of 2.85 eV,¹³ which does not need external conditions, such as strong electric field¹⁴ or doping¹⁵. Therefore, Cr_2C becomes a promising two-dimensional candidate for spintronic devices. It is noted that the half-metallicity requires atomically clean surfaces. When the surfaces are passivated, the half-metallicity of Cr_2C is suppressed.¹³ For the above titanium-containing MXenes, the magnetism also disappears when the bare surfaces are passivated.⁴⁻⁸ During etching process, for example with hydrofluoric acid,³ it is difficult to maintain such clean surfaces. This limits their application in spintronics. In the present work, another MXene Cr_2N , which has a different number of electrons in a unit cell with

Cr₂C, is investigated by using density functional theory. It is indicated that the bare Cr₂N is not half-metallic. On the contrary, half-metallicity appears when the surfaces are passivated by oxygen atoms.

MODELS AND COMPUTATIONAL DETAILS

The Cr₂N MXene is assumed to be exfoliated from parent Cr₂GaN. During the supposed treatment with hydrofluoric acid, the Ga atoms should be replaced by F or OH. On the other hand, Cr₂GaN is also observed to extrude elemental Ga at room temperature. Gases, such as O₂, are assumed to replace the Ga in the basal plane.¹⁶ Thus the bare Cr₂N and the surface-passivated Cr₂NT₂ (T=F, OH or O) are investigated.

As shown in Figure 1a,b, two-dimensional bare Cr₂N has a hexagonal layered structure and the N atom layer is sandwiched between the two layers of the Cr atoms. The Cr atoms in different layers are marked with different colors. Both ferromagnetic (FM) and anti-ferromagnetic (AFM) configurations are considered in the calculations, which are shown in Figure 1c-h. In the FM, AFM2 and AFM4 configurations, the spins in the different Cr layers are parallel to each other. On the contrary, the spins in the different Cr layers are anti-parallel in the AFM1, AFM3 and AFM5 configurations. As denoted by tetragons in Figure 1c-h, only the primitive cell is needed for FM and AFM1 configurations. A 2×1 unit cell is constructed for calculating AFM2 and AFM3 configurations, while a 2×2 unit cell is used to calculate AFM4 and AFM5 configurations.

The geometrical optimization and the electronic properties calculations are performed by the VASP program.¹⁷ The PBE density functional¹⁸ and the projector-augmented wave basis with an energy cutoff of 400 eV are used. In order to describe the strongly correlated 3d electrons of Cr atoms, the GGA+U method is used. In this framework, the difference between the onsite coulomb (U) and exchange (J) parameters is set to 3 eV (U-J). This value is successfully applied to similar systems, such as CrO₂¹⁹ and CrC₂¹³. A 41×41×1 Monkhorst-Pack k-point sampling is used in the first Brillouin zone of the hexagonal unit cell. The vacuum layer is around 15 Å in order to avoid possible

interaction between images. The HSE06 hybrid density functional,²⁰ which can accurately describe the properties of solids,²¹ is also used to confirm the energies and electronic properties obtained by the GGA+U method. In order to further verify the stability, the phonon dispersion is obtained through density functional perturbation theory with the aid of Phonopy code,²² which is based on a 4×4 supercell.

Besides the infinitely long structures, electronic devices with size of nanometer are also investigated based on the non-equilibrium Green's function method. The current-bias characteristics is obtained through the Landauer-Büttiker formula²³ by using the OPENMX program²⁴

$$I = \frac{e}{h} \int_{-\infty}^{+\infty} T(E, V_b) [f_L(E) - f_R(E)] dE$$

in which $T(E, V_b)$ is a transmission coefficient at energy E and bias V_b , $f_L(E)$ and $f_R(E)$ are Fermi-Dirac distribution functions for left and right electrodes. Two-dimensional rectangular unit cell is constructed, which is composed of two primitive cells. The left and right electrodes are composed of two unit cells while the scattering region is composed of three unit cells. Norm-conserving pseudopotentials²⁵ and variationally optimized pseudo-atomic localized basis functions^{26, 27} are used in this program. Each s, p or d (for Cr atom) orbital is described by a primitive orbital. Default convergence criterions are used in the calculation. The self-consistent field iteration stops when the absolute energy deviation between the current and the previous step is less than 10^{-6} Hartree. The energy cutoff is 150 Ry and 121 k-points are used along the transport direction. The GGA+U method (the PBE density functional with U-J=3 eV) is also available in this program. For consistency, the results are all obtained by the GGA+U method unless explicitly stated.

RESULTS AND DISCUSSION

For the FM configuration, the optimized bond length between the Cr and N atoms is 2.13 Å. In its band structures shown in Figure 2a, there are bands going across the Fermi level

for both spins. It is a metal, but not a half-metal. The number of electrons in a N atom is bigger than that in a C atom, so the band structures are different from those of the half-metallic Cr_2C .¹³ The unbalanced band structures for both spins imply magnetic properties. The total magnetic moment is $8.61 \mu_{\text{B}}$. Detailed analysis indicates that the magnetism is mainly located on Cr atoms. Each Cr atom has a magnetic moment of $4.45 \mu_{\text{B}}$, while that on a N atom is $-0.30 \mu_{\text{B}}$. These values are not integers, which are different from those of Cr_2C .¹³ In order to elucidate the fractional magnetic moment, Bader charge analysis²⁸⁻³⁰ is performed. The net charge on a N atom is $-1.50 |e|$. Unlike the C atom in Cr_2C , the N atom with fractional charges possesses non-zero magnetic moment. The Cr atom with a formal fractional charge $+0.75$ also has a fractional magnetic moment.

The relative energies of the optimized FM, AFM1, AFM2, AFM3, AFM4 and AFM5 structures are 203, 301, 175, 0, 1394 and 1568 meV, respectively. This indicates that Cr_2N has an AFM3 ground state. There are two types of bond lengths (2.07 and 2.15 Å) in the optimized AFM3 structure. The symmetry breaking and geometrical distortion introduce stronger bonds, especially for the Cr and N atoms with distance of 2.07 Å, which introduces additional stability. It should be noted that the initial hypothetical AFM4 and AFM5 configurations shown in Figure 1g,h have never been obtained by various initial structures. This indicates that the structures with so many anti-ferromagnetic couplings are not stable. The structures either converges to the most stable AFM3 configurations, or to the nominal AFM4 and AFM5 configurations shown in Figure 1i,j. In the nominal AFM4 and AFM5 configurations, the spins are localized on only a few Cr atoms in the distorted structures. The absence of the magnetism on the other Cr atoms makes the two nominal configurations very unstable. Only AFM1, AFM2 and AFM3 configurations are normal AFM states.

All the above AFM Cr_2N structures have anti-ferromagnetic band structures. Only those of the most stable AFM3 structures are shown in Figure 3a. Since the band structures for majority and minority spins are degenerate, only those for the majority spin

are shown. In the band structures, two bands go across the Fermi level, indicating metallic characteristics. Many AFM structures are non-metallic. Two-dimensional Cr₂N is an AFM metal, which should be useful in spintronics. However, the bare surfaces can be passivated during etching process. Its electronic properties may change after surface-passivation.

The hybrid density functional HSE06 is also used to confirm the results based on the GGA+U method. In the FM configuration, the bond length is 2.10 Å, close to the GGA+U result (2.13 Å). The total magnetic moment is 8.59 μ_B, also close to the GGA+U result (8.61 μ_B). The relative energies per primitive cell of the optimized FM, as well as the normal AFM1, AFM2 and AFM3 structures are 295, 336, 130 and 0 meV. AFM3 configuration is also the ground state. The optimized AFM3 structure also has two types of bond lengths (2.04 and 2.11 Å). The HSE06 density functional indicates that the two-dimensional Cr₂N is an AFM metal. The results obtained by the HSE06 density functional are consistent with those obtained by the GGA+U method.

In the surface-passivated structures, the functional atoms or groups are above the hollow site of the N atoms and pointed to the Cr atoms in the opposite layer.^{8, 11} The relative energies per primitive cell of the optimized FM, AFM1, AFM2, AFM3, AFM4 and AFM5 structures are 58, 543, 200, 0, 3890 and 1538 meV for Cr₂NF₂, 38, 260, 149, 0, 1427 and 1391 meV for Cr₂N(OH)₂, 0, 80, 220, 264, 1782 and 2609 meV for Cr₂NO₂. Similar to the situation of Cr₂N, the nominal AFM4 and AFM5 configurations are very unstable for the surface-passivated structures. From bare Cr₂N to the mono-valent functional group-passivated Cr₂NF₂ and Cr₂N(OH)₂, the AFM3 configurations are always the ground states. However, the divalent oxygen atom-passivated Cr₂NO₂ has a FM ground state.

The band structures of Cr₂NF₂ and Cr₂N(OH)₂ with stable AFM3 configurations shown in Figure 3b,c are quite similar to those of Cr₂N. Although the AFM3 configuration is not the ground state of Cr₂NO₂, the band structures are also shown in Figure 3d for

comparison. Like the other AFM3 structures, there are two bands going across the Fermi level in the band structures of Cr_2NO_2 . The four configurations are all AFM metals.

As shown in Figure 2d, the band structures of Cr_2NO_2 with FM ground state indicate that it is a half-metal. It is metallic for majority spin and semiconducting for minority spin. Actually, the band structures of Cr_2NF_2 and $\text{Cr}_2\text{N}(\text{OH})_2$ with FM configuration (shown in Figure 2b,c) also have this half-metallic characteristics. As shown in Figure 2a, the bare Cr_2N with FM configuration is metallic for both spins. After the surface-passivations, the total magnetic moments in the FM configurations drops from 8.61 to 7.00 μ_B both for Cr_2NF_2 and $\text{Cr}_2\text{N}(\text{OH})_2$. The magnetic moment on each Cr atom is 3.59 μ_B . The magnetic moment on the N atom is -0.23 μ_B , while it is 0.02 or 0.01 μ_B on each F or O atom. Compared with Cr_2N , the magnetic moment on the Cr atom reduces by about 1 μ_B (from 4.45 to 3.59 μ_B). This is attributed to the surface-passivation by mono-valent functional atoms or groups. For the divalent oxygen atom-passivated Cr_2NO_2 , the total magnetic moment reduces further to 5.00 μ_B . The magnetic moment on each Cr atom is 2.76 μ_B , while that on each N or O atom is -0.18 or -0.17 μ_B . With the functional atoms or groups, the electrons with minority spin at the Fermi level are suppressed in the FM configuration of Cr_2N . From Cr_2N to Cr_2NF_2 , $\text{Cr}_2\text{N}(\text{OH})_2$ and then to Cr_2NO_2 , the total magnetic moments and those on each Cr atom drop. The relative energies of the FM configurations with respect to the corresponding AFM3 configurations decrease from 203 to 58 and 38 meV for Cr_2N , Cr_2NF_2 and $\text{Cr}_2\text{N}(\text{OH})_2$. Finally, the FM configuration becomes the ground state of Cr_2NO_2 . A possible route to obtain Cr_2NO_2 is extruding elemental Ga from Cr_2GaN at room temperature.¹⁶ In the etching technology, Cr_2NO_2 is assumed to be obtained by a post treatment of the resulting $\text{Cr}_2\text{N}(\text{OH})_2$. The energy change of the reaction $\text{Cr}_2\text{N}(\text{OH})_2 + 1/2 \text{O}_2 \rightarrow \text{Cr}_2\text{NO}_2 + \text{H}_2\text{O}$ is -1.7 eV, indicating that this process is energetically favorable.

For the half-metallic Cr_2NO_2 , the HSE06 density functional is also used to confirm the result obtained by the GGA+U method. After geometrical optimization, the band

structures shown in Figure 2e are quite similar to those in Figure 2d. The half-metallicity of Cr_2NO_2 maintains. There are still two bands going across the Fermi level only for majority spin. The half-metallicity is intrinsic and it does not need external strong electric field or doping.^{14, 15} And more importantly, Cr_2NO_2 is surface-passivated and is more likely to be realized than the bare structure. Therefore, the surface-oxygen-passivated Cr_2N MXene should be a promising candidate for spintronics. The indirect band gap of Cr_2NO_2 for minority spin is 2.79 or 3.88 eV under the GGA+U or HSE06 method. The large band gap implies sustainable half-metallicity during device operation.

The size of an electronic device becomes progressively smaller with increasing time. It is interesting to see whether the half-metallicity is sustainable when bias is applied to nanometer sized devices. The transmission spectrum at zero bias of the Cr_2NO_2 device is shown in Figure 4a. In such a narrow device, the transmission for minority spin is still absent and the half-metallicity maintains. As shown in Figure 4b, the current for majority spin or the total current increases with the increasing bias until the bias reaches 0.5 V. Then the current is saturated when the bias increases further to 1 V. The spin polarization is always 100% at this bias range. The half-metallicity of the Cr_2NO_2 is still robust when a wide range of bias is applied to the device. The current at 0.5 V is 19.7 μA , corresponding to a high conductance of 39.4 μS . The nanometer sized Cr_2NO_2 device is highly conductive and has an 100% spin polarization. It should be a good candidate for spintronic devices.

Since Cr_2NO_2 has appealing properties, its phonon dispersion is calculated. As shown in Figure 5, no non-trivial imaginary frequency is found. The imaginary frequencies (no more than 3 cm^{-1}) near the Γ points are attributed to the three translational modes. Because of the numerical method adopted by density functional theory, the frequencies of the translational modes are not exactly zero. The phonon dispersion verifies the stability of Cr_2NO_2 . Ab initio molecular dynamics simulations are also performed. The VASP program currently can only perform constant volume molecular dynamics. A micro

canonical ensemble is used for the four stable configurations. A 2×2 unit cell is used and the simulation temperature is set to 300 K. The step size is set to 1 fs. During the 5000 simulation steps, no essential structural deformation is found except the orientation of the hydrogen atoms in $\text{Cr}_2\text{N}(\text{OH})_2$. In Figure 6a-d, the energy fluctuation ranges are 193, 264, 412 and 368 meV per primitive cell for Cr_2N , Cr_2NF_2 , $\text{Cr}_2\text{N}(\text{OH})_2$ and Cr_2NO_2 , respectively. These values are higher than the energy differences between different corresponding configurations. However, the transition between different configurations does not occur during the molecular dynamics simulations. This confirms the stabilities of Cr_2NO_2 with FM configuration, as well as Cr_2N , Cr_2NF_2 and $\text{Cr}_2\text{N}(\text{OH})_2$ with AFM3 configurations. The highest energy fluctuation range for $\text{Cr}_2\text{N}(\text{OH})_2$ should be attributed to the random orientation of the hydrogen atoms in the molecular dynamics simulation. Although the AFM3 ground state of Cr_2N is generally unchanged, the total magnetic moment changes slightly. As shown in Figure 6e, the total magnetic moment oscillates up and down. The amplitude is in a rough range of 0.2-0.6 μ_B . After the surface-passivation by mono-valent F atoms or OH groups, the oscillation becomes much weaker. In Figure 6f, the total magnetic moment of Cr_2NF_2 is always zero except a very small deviation of -0.01 μ_B around 3919 fs. The magnetic configuration is much more stable than that of the bare Cr_2N . For $\text{Cr}_2\text{N}(\text{OH})_2$, the largest deviation as shown in Figure 6g is -0.11 μ_B and this value is much smaller than that of the bare Cr_2N . The slightly stronger oscillation compared to Cr_2NF_2 should be also attributed to the random orientation of the hydrogen atoms. For the divalent oxygen atom-passivated Cr_2NO_2 , the total magnetic moment as shown in Figure 6h is unchanged. The molecular dynamics simulations also indicate that the surface-passivation, especially the surface oxygen atom-passivation stabilizes the total magnetic configurations of the Cr_2N MXenes.

CONCLUSIONS

Two-dimensional Cr_2N MXene as well as the surface-passivated MXenes are investigated by using density functional theory. The bare Cr_2N MXene is an AFM metal. The

surface-passivated Cr_2NF_2 and $\text{Cr}_2\text{N}(\text{OH})_2$ are also AFM metals, while Cr_2NO_2 is a half-metal. The number of electrons in Cr_2N is different from that in Cr_2C . Unlike Cr_2C that is a half-metal, the FM configuration of the Cr_2N is metallic for both spins. After surface-passivation, the electrons with minority spin at the Fermi level are suppressed and the MXenes with FM configurations have half-metallic band structures. From the bare Cr_2N to the mono-valent atom or functional group-passivated Cr_2NF_2 and $\text{Cr}_2\text{N}(\text{OH})_2$, and then to the divalent oxygen atom-passivated Cr_2NO_2 , the FM configuration becomes more and more stable. Finally, Cr_2NO_2 has a FM ground state. The half-metallicity of the Cr_2NO_2 MXene is intrinsic, which does not require external electric field or doping. Because it has a large band gap of 2.79 eV for minority spin, the half-metallicity is even robust when bias is applied to the nanometer sized Cr_2NO_2 device. Unlike the Cr_2C , the half-metallicity here does not require atomically clean surfaces. The Cr_2NO_2 MXene is a surface-passivated stable structure. Therefore, the surface-oxygen-passivated Cr_2N MXene should be a promising candidate for spintronics.

REFERENCES

- (1) Barsoum, M. W. *MAX phases properties of machinable ternary carbides and nitrides*; Wiley-VCH Verlag GmbH & Co. KGaA: Weinheim, Germany, 2013.
- (2) Novoselov, K.S.; Jiang, D.; Schedin, F.; Booth, T. J.; Khotkevich, V. V.; Morozov, S. V.; Geim, A. K. Two-Dimensional Atomic Crystals. *Proc. Natl. Acad. Sci. USA* **2015**, *102*, 10451–10453.
- (3) Naguib, M.; Kurtoglu, M.; Presser, V.; Lu, J.; Niu, J.; Heon, M.; Hultman, L.; Gogotsi, Y.; Barsoum, M. W. Two-Dimensional Nanocrystals Produced by Exfoliation of Ti_3AlC_2 . *Adv. Mater.* **2011**, *23*, 4248–4253.
- (4) Naguib, M.; Mochalin, V. N.; Barsoum, M. W.; Gogotsi Y. 25th Anniversary Article: MXenes: A New Family of Two-Dimensional Materials. *Adv. Mater.* **2014**, *26*, 992–1004.
- (5) Shein, I. R.; Ivanovskii, A. L. Graphene-Like Titanium Carbides and Nitrides $\text{Ti}_{n+1}\text{C}_n$,

Ti_{n+1}N_n (n = 1, 2, and 3) from De-Intercalated MAX Phases: First-Principles Probing of Their Structural, Electronic Properties and Relative Stability. *Comput. Mater. Sci.* **2012**, *65*, 104–114.

(6) Tang, Q.; Zhou, Z.; Shen, P. Are MXenes Promising Anode Materials for Li Ion Batteries? Computational Studies on Electronic Properties and Li Storage Capability of Ti₃C₂ and Ti₃C₂X₂ (X = F, OH) Monolayer. *J. Am. Chem. Soc.* **2012**, *134*, 16909–16916.

(7) Wu, F.; Luo, K.; Huang, C.; Wu, W.; Meng, P.; Liu, Y.; Kan, E. Theoretical Understanding of Magnetic and Electronic Structures of Ti₃C₂ Monolayer and Its Derivatives. *Solid State Commun.* **2015**, *222*, 9–13.

(8) Xie, Y.; Kent, P. R. C. Hybrid Density Functional Study of Structural and Electronic Properties of Functionalized Ti_{n+1}X_n (X = C, N) Monolayers. *Phys. Rev. B* **2013**, *87*, 235441.

(9) Gao, G.; Ding, G.; Li, J.; Yao, K.; Wu, M.; Qian, M. Monolayer MXenes: Promising Half-Metals and Spin Gapless Semiconductors. *Nanoscale* **2016**, *8*, 8986–8994.

(10) Lane, N. J.; Barsoum, M. W.; Rondinelli, J. M. Correlation Effects and Spin-Orbit Interactions in Two-Dimensional Hexagonal 5d Transition Metal Carbides, Ta_{n+1}C_n (n = 1, 2, 3). *EPL* **2013**, *101*, 57004.

(11) Khazaei, M.; Arai, M.; Sasaki, T.; Chung, C.-Y.; Venkataramanan, N. S.; Estili, M.; Sakka, Y.; Kawazoe, Y. Novel Electronic and Magnetic Properties of Two-Dimensional Transition Metal Carbides and Nitrides. *Adv. Funct. Mater.* **2013**, *23*, 2185–2192.

(12) Zhao, S.; Kang, W.; Xue, J. MXene nanoribbons. *J. Mater. Chem. C* **2015**, *3*, 879–888.

(13) Si, C.; Zhou, J.; Sun, Z. Half-Metallic Ferromagnetism and Surface Functionalization-Induced Metal–Insulator Transition in Graphene-Like Two-Dimensional Cr₂C Crystals. *ACS Appl. Mater. Interfaces* **2015**, *7*, 17510–17515.

(14) Son, Y.-W.; Cohen, M. L.; Louie, S. G. Half-Metallic Graphene Nanoribbons. *Nature* **2006**, *444*, 347–349.

- (15) Li, X.; Wu, X.; Yang, J. Room-Temperature Half-Metallicity in La(Mn,Zn)AsO Alloy via Element Substitutions. *J. Am. Chem. Soc.* **2014**, *136*, 5664–5669.
- (16) Barsoum, M. W.; Farber, L. Room-Temperature Deintercalation and Self-Extrusion of Ga from Cr₂GaN. *Science* **1999**, *284*, 937–939.
- (17) Kresse, G.; Furthmüller, J. Efficient Iterative Schemes for ab initio Total-Energy Calculations using a Plane-Wave Basis Set. *Phys. Rev. B* **1996**, *54*, 11169.
- (18) Perdew, J. P.; Burke, K.; Ernzerhof, M. Generalized Gradient Approximation Made Simple. *Phys. Rev. Lett.* **1996**, *77*, 3865.
- (19) Korotin, M. A.; Anisimov, V. I.; Khomskii, D. I.; Sawatzky, G. A. CrO₂: a Self-doped Double Exchange Ferromagnet. *Phys. Rev. Lett.* **1998**, *80*, 4305.
- (20) Krukau, A. V.; Vydrov, O. A.; Izmaylov, A. F.; Scuseria, G. E. Range-Separated Local Hybrids. *J. Chem. Phys.* **2006**, *125*, 224106.
- (21) Henderson, T. M.; Paier, J.; Scuseria, G. E. Accurate treatment of solids with the HSE screened hybrid. *Phys. Status Solidi B* **2011**, *248*, 767-774.
- (22) Togo, A.; Oba, F.; Tanaka, I. First-Principles Calculations of the Ferroelastic Transition between Rutile-Type and CaCl₂-Type SiO₂ at High Pressures. *Phys. Rev. B* **2008**, *78*, 134106.
- (23) Büttiker, M.; Imry, Y.; Landauer, R.; Pinhas, S. Generalized Many-Channel Conductance Formula with Application to Small Rings. *Phys. Rev. B* **1985**, *31*, 6207.
- (24) <http://www.openmx-square.org/>.
- (25) Morrison, I.; Bylander, D. M.; Kleinman, L. Nonlocal Hermitian Norm-Conserving Vanderbilt Pseudopotential. *Phys. Rev. B* **1993**, *47*, 6728.
- (26) Ozaki, T. Variationally Optimized Atomic Orbitals for Large-Scale Electronic Structures. *Phys. Rev. B* **2003**, *67*, 155108.
- (27) Ozaki, T.; Kino, H. Numerical Atomic Basis Orbitals from H to Kr. *Phys. Rev. B* **2004**, *69*, 195113.
- (28) Henkelman, G.; Arnaldsson, A.; Jónsson, H. A Fast and Robust Algorithm for

Bader Decomposition of Charge Density. *Comput. Mater. Sci.* **2006**, *36*, 354–360.

(29) Sanville, E.; Kenny, S.; Smith, R.; Henkelman, G. Improved Grid-Based Algorithm for Bader Charge Allocation. *J. Comput. Chem.* **2007**, *28*, 899–908.

(30) Tang, W.; Sanville, E.; Henkelman, G. A Grid-Based Bader Analysis Algorithm without Lattice Bias. *J. Phys.: Condens. Matter* **2009**, *21*, 084204.

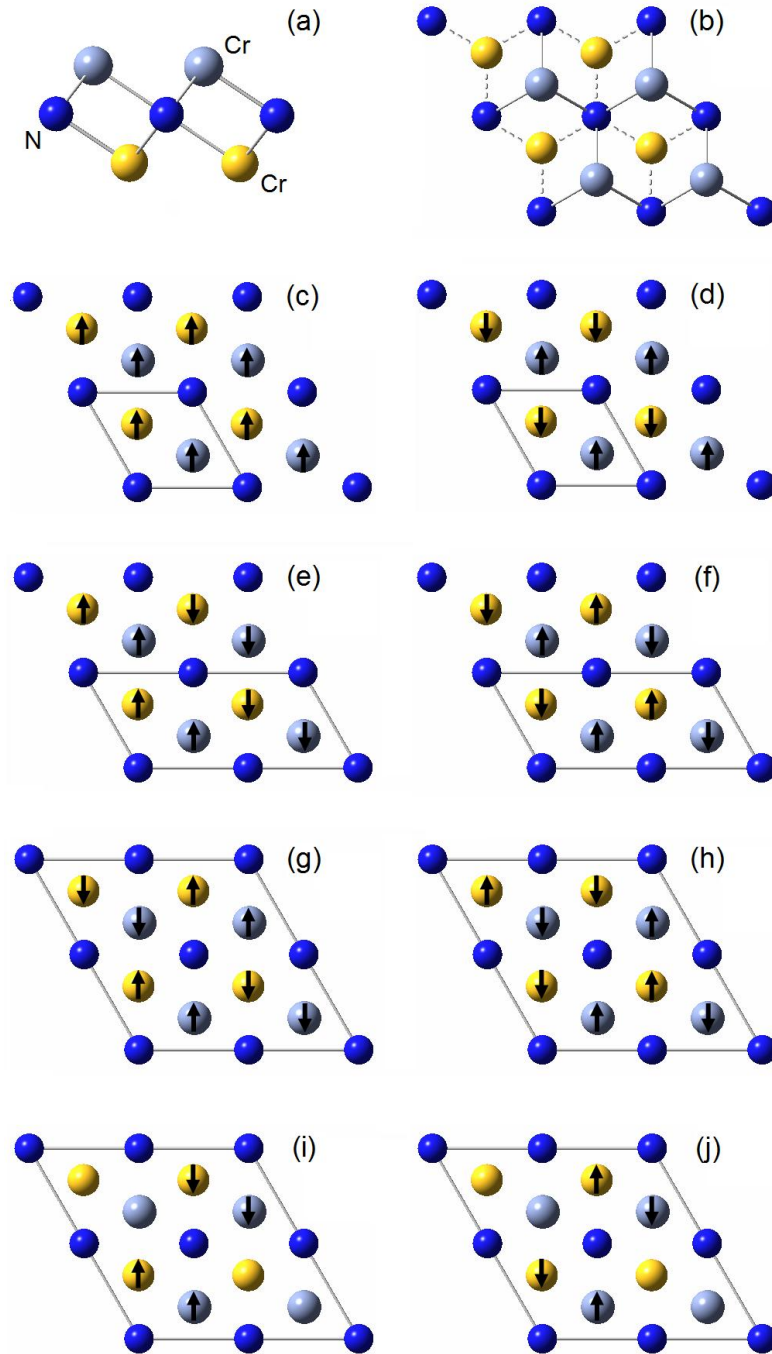


Figure 1. (a) Side and (b) top view of two-dimensional Cr_2N , (c) FM, (d) AFM1, (e) AFM2 and (f) AFM3 configurations, (g) initial guess of AFM4 and (h) AFM5 configurations, (i) AFM4 and (j) AFM5 configurations for the optimized structures. The adopted unit cells are denoted by tetragons in (c)-(j). The Cr atoms in different layers are labeled with different colors.

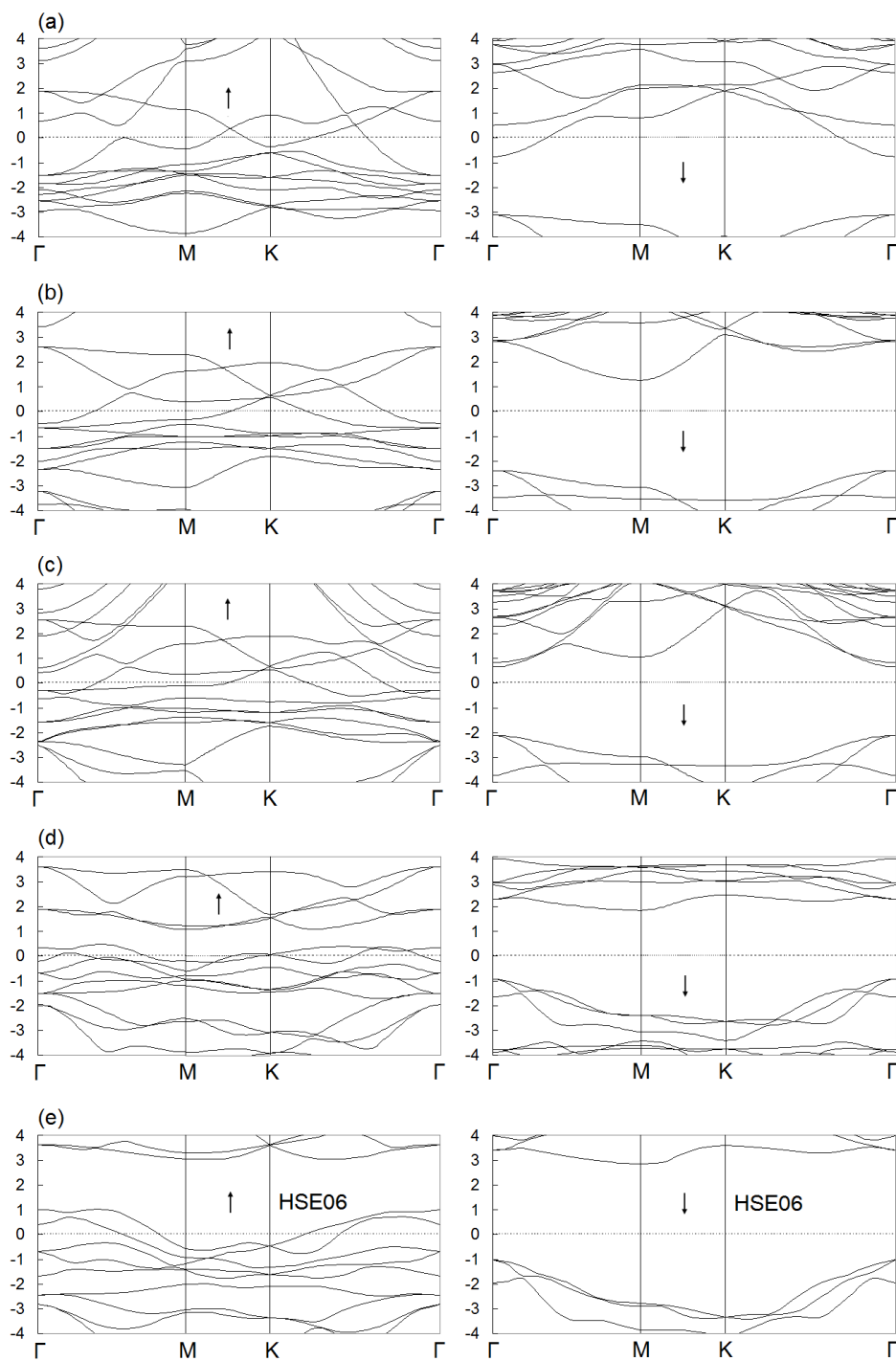


Figure 2. Band structures of (a) Cr_2N , (b) Cr_2NF_2 , (c) $\text{Cr}_2\text{N}(\text{OH})_2$ and (d) Cr_2NO_2 with FM configurations, (e) band structures of Cr_2NO_2 with FM configurations obtained by the HSE06 density functional. Vertical axis: energy in eV, horizontal axis: reciprocal lattice vector.

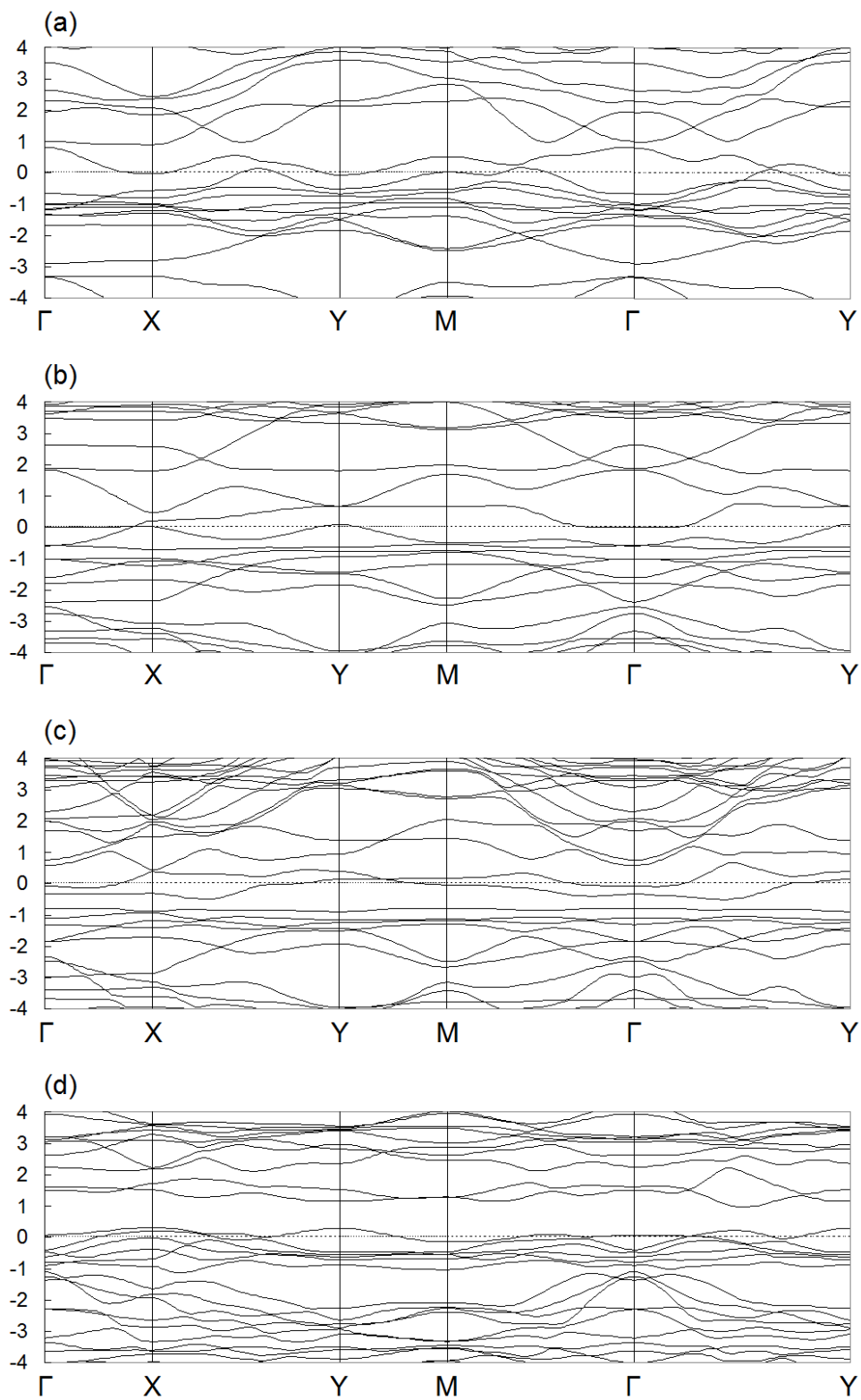


Figure 3. Band structures of (a) Cr_2N , (b) Cr_2NF_2 , (c) $\text{Cr}_2\text{N}(\text{OH})_2$ and (d) Cr_2NO_2 with AFM3 configurations. Vertical axis: energy in eV, horizontal axis: reciprocal lattice vector.

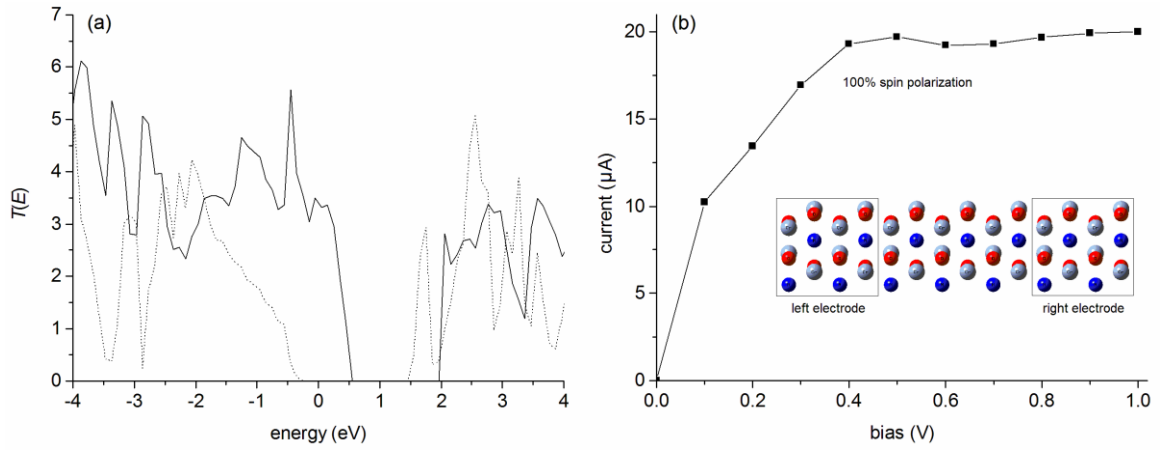


Figure 4. (a) Transmission spectrum and (b) current-bias curve of the Cr_2NO_2 device, structure of the device is in the inset.

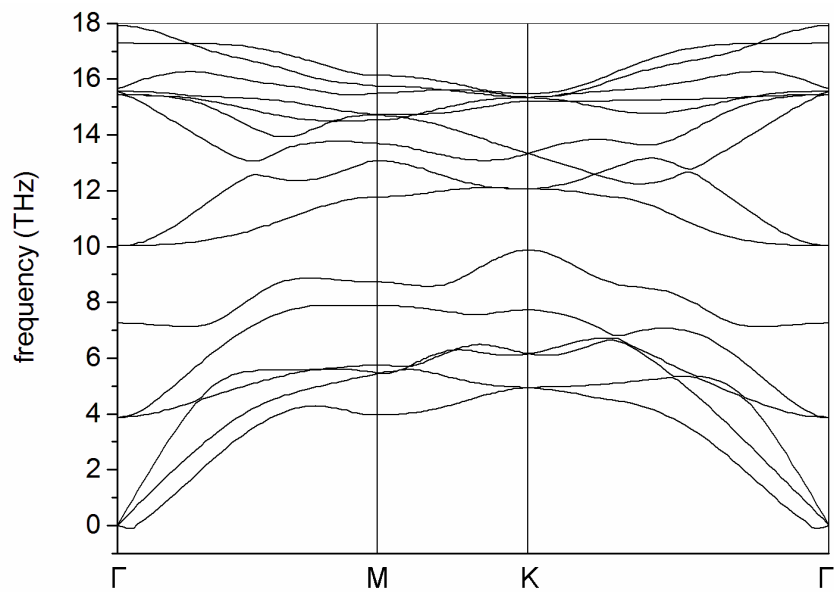


Figure 5. (a) Phonon dispersion of Cr_2NO_2 with FM configuration.

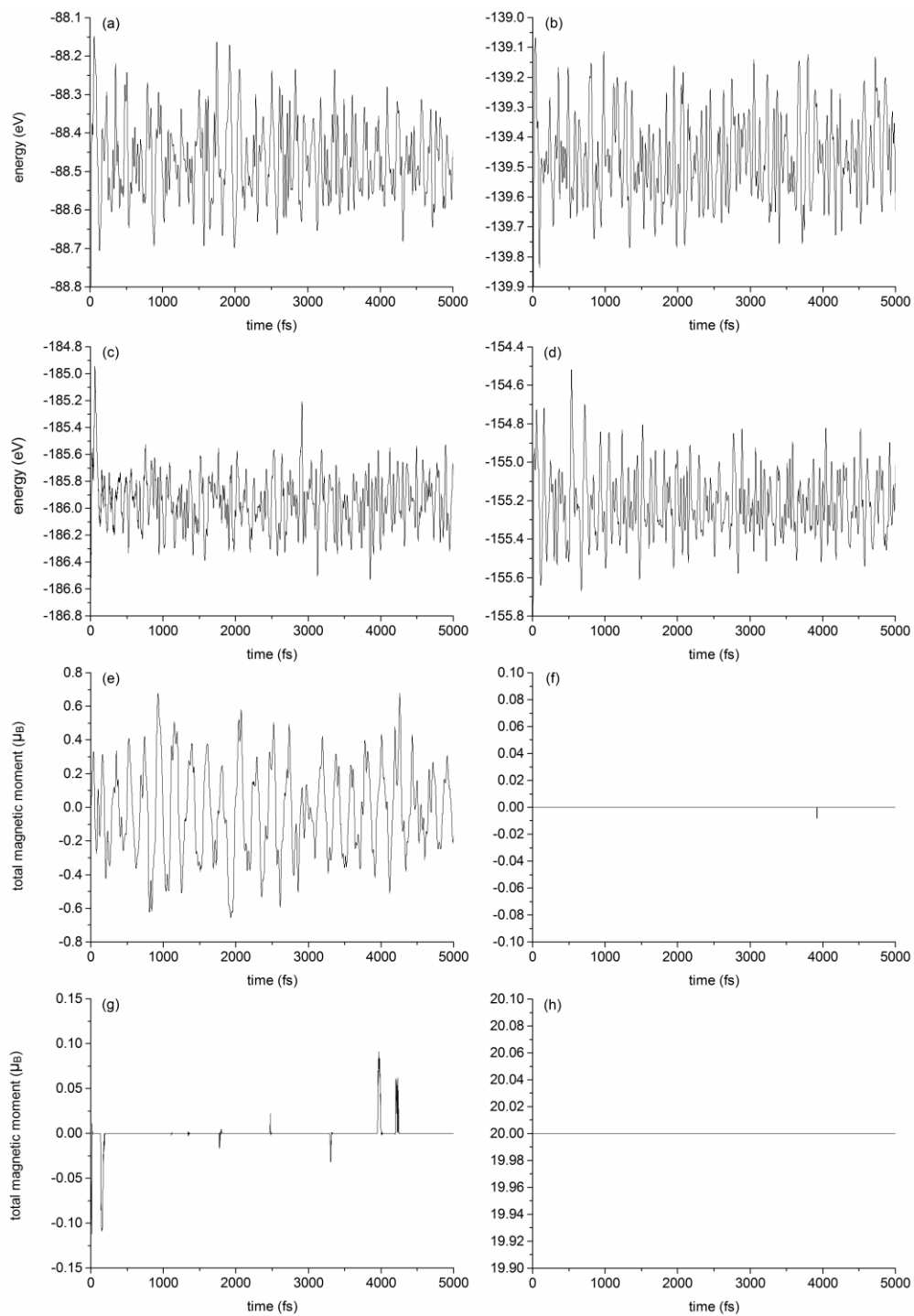


Figure 6. Energy fluctuation of (a) Cr₂N (b) Cr₂NF₂, (c) Cr₂N(OH)₂, (d) Cr₂NO₂ and total magnetic moments of (e) Cr₂N (f) Cr₂NF₂, (g) Cr₂N(OH)₂, (h) Cr₂NO₂ during molecular dynamic.